



A Dendrite-Free Lithium Metal Battery by Incorporating Poly(dimethylsiloxane) Layer onto the Porous Three-Dimensional Copper Current Collector

Jihyeok Song¹ · Subin Lee^{2,3} · Youngkwang Kim⁴ · Yung-Eun Sung^{1,5} · Taeun Yim^{2,3} · Oh Joong Kwon⁴

Received: 22 April 2024 / Revised: 12 July 2024 / Accepted: 23 July 2024

© The Author(s), under exclusive licence to Korean Institute of Chemical Engineers, Seoul, Korea 2024

Abstract

As an anode, lithium metal electrode is one of the most promising candidates for lithium batteries because of their theoretically high specific capacity and low redox potential. However, lithium dendrites are formed during the cycle of lithium deposition and dissolution on the copper current collector during charging and discharging, threatening the stability and durability of lithium metal batteries (LMBs). In this study, a three-dimensional (3D) porous copper coated with a polymer layer (polydimethylsiloxane, PDMS) is used as a current collector to ensure high stability. A PDMS-coated 3D porous current collector is prepared by Cu electrodeposition using hydrogen bubbles as a template followed by a PDMS coating. PDMS coating is performed by spin coating of PDMS on a slide glass and transferring it to the current collector. The 3D current collector functionalized by PDMS offers prolonged lifespans in both Li deposition/dissolution and intercalation of the lithium iron phosphate cathode, as the functionalized PDMS-coated 3D porous current collector effectively prevents the growth of Li dendrites at the interface.

Keywords Lithium metal anode · 3D current collector · Cu foam · Polydimethylsiloxane · Dendrite free · Lithium metal battery

Jihyeok Song and Subin Lee contributed equally to this work.

✉ Taeun Yim
yte0102@inu.ac.kr

✉ Oh Joong Kwon
ojkwon@inu.ac.kr

¹ School of Chemical and Biological Engineering, Seoul National University, Seoul 08826, Republic of Korea

² Advanced Batteries Laboratory, Department of Chemistry, Incheon National University, 119 Academy-ro, Yeonsu-gu, Incheon 22012, Republic of Korea

³ Research Institute of Basic Sciences, College of Natural Science, Incheon National University, 119 Academy-ro, Yeonsu-gu, Incheon 22012, Republic of Korea

⁴ Department of Energy and Chemical Engineering and Innovation Centre for Chemical Engineering, Incheon National University, 119 Academi-ro, Yeonsu-gu, Incheon 22012, Republic of Korea

⁵ Center for Nanoparticle Research, Institute for Basic Science (IBS), Seoul 08826, Republic of Korea

Introduction

Interest in renewable and sustainable energy storage and conversion technologies has increased as a consequence of global warming. Secondary batteries, which can be charged and discharged semi-permanently using lithium or zinc redox processes, are an efficient energy storage technology [1–3]. This battery technology is receiving significant attention due to its high power density and low storage cost, which resolve the huge energy production fluctuations of new and renewable energy technologies. However, except for mobile devices and automobiles, battery energy density does not meet the needs of large-scale industries. In this regard, the lithium metal anode has received interest as a next-generation battery technology because it has a high theoretical capacity of 3860 mA h g⁻¹ and the lowest redox potential of -3.04 V vs. a standard hydrogen electrode [1–7]. However, the formation of lithium dendrites while repeating the deposition–dissolution process diminishes the long-term performance of the battery and increases the risk of explosion in lithium metal batteries (LMBs) [1–8].

Many studies have attempted to employ lithium metal as an anode in various ways. A method to modify the solid electrolyte interface (SEI) with a stable and flexible solid or polymer layer has been studied, and this protective layer has proven effective in preventing lithium dendrite growth [9]. The method of covering lithium metal with a Li-ion conductive polymer [10–13], Li-F [14, 15], or Li-based alloy [16, 17] demonstrated reduced damage to the SEI and excellent durability as lithium deposition was induced inside the SEI. Another approach is to deposit lithium metal onto a porous structure [18–21]. Zheng et al. formed a polymer layer on a spherical template, carbonized it, and removed the template to obtain a hollow carbon sphere [18]. The volume change during lithium deposition and dissolution was minimized due to the porous structure and large surface area, enabling uniform lithium deposition. As a result, it showed higher stability than the planar structure during repeated deposition–dissolution processes of lithium in a long-term cycling experiment.

A method for developing a copper current collector with a three-dimensional porous structure, which has been frequently adopted in lithium ion batteries, has recently been reported to prevent lithium dendrite formation in LMBs [22–25]. Yang et al. reported a three-dimensional copper current collector that inhibited the growth of lithium dendrites during lithium deposition [23]. However, there were disadvantages in that it is difficult to fabricate a porous copper film, and the process is time-consuming for practical application. In a recent study, a simple and time-saving method was reported for forming a porous copper layer by electroplating copper using hydrogen bubbles as a template [26, 27]. The hydrogen bubbles generated during copper deposition play the role of the porous template and are removed spontaneously while copper forms a three-dimensional (3D) structure. The size of the hydrogen bubble depends on the deposition current density, thus the structure of 3D Cu foam can be manipulated with the control of the current density. Qiu et al. formed a porous copper film by electroplating and showed high stability even during long-term operation because lithium dendrite growth was inhibited. Electrochemical impedance spectroscopy revealed that the porous copper film induced a lower local current density than planar copper, resulting in uniform lithium plating [26].

The alleviating effect of the porous copper layer on lithium dendrite formation is attributed to sufficient lithium nucleation originating from a large surface area [23, 26–28]. When lithium is deposited, the porous copper layer induces a large amount of lithium nucleation over a large surface area, forming a uniform lithium layer. However, according to a recent study by Yun et al., lithium deposition on a porous copper film is not conducted uniformly over the entire area but is conducted intensively on the top. As a solution, lithium growth from the bottom through passivation

on the upper part of the porous copper layer has been suggested. The upper part was passivated using a polyvinylidene fluoride coating to hinder lithium deposition, and the lower part was activated using a silver coating to facilitate lithium deposition. The elaborately designed 3D framework electrodes with an interfacial activity gradient exhibited bottom-up deposition of lithium in the 3D current collector [29].

In this study, a porous copper current collector was prepared by electroplating copper using hydrogen bubbles as a template. Polydimethylsiloxane (PDMS) was applied to cover the upper surface of the porous copper film to prevent lithium deposition on the current collector's top. PDMS is a widely recognized polymer known for its high chemical resistance, even in organic electrolytes, making it a suitable choice for battery fabrication [4, 30]. In addition, PDMS is non-toxic and easy to handle, making itself well for straightforward applications. The PDMS coating was performed using a simple transfer process, which effectively prevented the top layer from accessing lithium, leading to lithium deposition only inside the porous current collector. This improved the stability of the LMB, which showed longer cyclability than other types of current collectors. The study revealed that covering the top of the porous current collector enabled lithium deposition from the bottom of the pores, thus proving the origin of stability of the LMBs assembled with a PDMS-coated porous current collector.

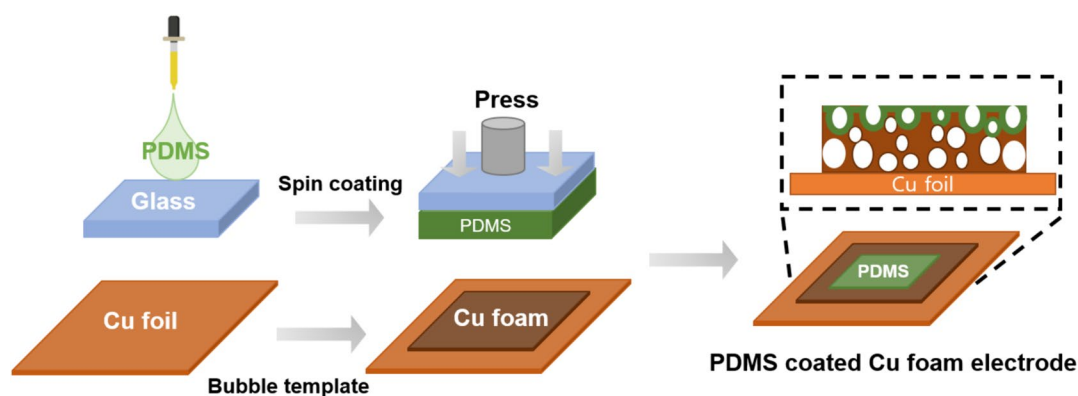
Experimental

Preparation of Porous Copper Current Collector

2.5 × 2.5 cm² Cu foil was used as a substrate to fabricate a porous 3D Cu current collector. Cu foil loaded in a homemade frame was used as the working electrode, and a Cu plate was adopted as the counter and reference electrodes simultaneously in a two-electrode system. The electrolyte was composed of 0.5 M H₂SO₄ and 0.25 M CuSO₄·5H₂O solutions. After electrodeposition for 8 s at a current density of 4 A cm⁻², the Cu foam was washed alternately several times with ethanol and deionized water to remove the residual solution in the Cu foam effectively [27].

Surface Passivation of Cu Foam with PDMS

1.8 × 1.8 cm² cover glass was used as a substrate to prepare a PDMS layer. PDMS solution (SYLGARD™ 184 Silicone Elastomer Base, Dow Corning, USA) was coated on the cover glass by a spin coater (Rhabdos, SC-100RPM, South Korea) under 1600, 4500, 6000, and 8000 revolutions per minute (rpm) for 30 s. Subsequently, a curing agent (SYLGARD™ 184 Silicone Elastomer curing agent, Dow Corning, USA) was applied at 1000 rpm for 20 s, and the cover



Scheme 1 Schematic diagram showing the fabrication process of p-Cu foam

glass was stored in a vacuum for 72 h. Then the PDMS-coated cover glass and Cu foam were placed facing each other and pressed by a 5 g flat plastic plate and 10 g pendulums for 1 min, respectively. The pressure was calculated to be 4.63 g cm^{-2} . The fabricated electrodes coated with PDMS solution are denoted as p-Cu 1600, 4500, 6000, and 8000, respectively.

Cell Assembly and Electrochemical Operation

The cells were assembled with Cu foam as the working electrode, a Li anode (200 μm) as the counter and reference electrodes, (polyethylene) (PE) separator, and an electrolyte (1,2-dimethoxyethane (DME; Aldrich):1,3-dioxolane (DOL; Aldrich) = 8:2 (v/v%) + 1.0 M lithium bis(trifluoromethanesulfonyl)imide (LiTFSI; Soulbrain). For evaluating the Li plating/stripping, the cells were charged/discharged by a cycler (Wonatech): 2.0 mA h cm^{-2} Li metal was electrodeposited at 2.0 mA cm^{-2} onto the Cu foam substrate and then stripped until the potential of the cells reached a cutoff voltage of 0.5 V in each cycle. The internal resistance of the cells was measured via electrochemical impedance spectroscopy (EIS) using a potentiostat (VSP, Biologic) with an amplitude of 5 mV in the frequency range of 1 MHz–1 mHz. To analyze the behaviors of Li deposition, a Cu foam/Li metal half-cell was assembled, and the deposition and stripping of Li were measured. Then Cu foam and p-Cu 6000 were recovered and analyzed by optical microscope (BX53M, OLYMPUS).

For full-cell evaluation, LiFePO_4 (LFP; Aleees), cathodes were prepared as follows. 0.2 g of poly(vinylidene fluoride) (PVDF; Kureha) was dispersed in the 3.0 mL of *N*-methyl pyrrolidone (NMP; Ashland), and 0.2 g of conducting agent (Super-C; C-ENERGY) was added to the solution. The mixture was then agitated for 12 min using a paste mixer (PDM-300, KM Tech). Then 1.6 g of LFP cathode material was added to the solution and agitated for 12 min. The slurry was

cast onto the Al current collector, and it was dried for 12 h in a vacuum oven at 120 $^{\circ}\text{C}$. The loading density of the LFP cathode was 1.17 mg cm^{-2} , and the electrode density was 0.36 g cm^{-3} . The full cells were assembled with the cycled Cu foam (evaluated by Li plating/stripping for 50 cycles, diameter of 14 mm) as an anode, LFP cathode (diameter of 12 mm), PE separator, and 100 μL of electrolyte. The cells were cycled from 2.5 V (vs. Li/Li^+) to 4.0 V (vs. Li/Li^+) at a 0.1 C-rate (1.0 C: 150 mA g^{-1}) at room temperature (25 $^{\circ}\text{C}$).

Material Characterization

The morphologies of Cu foams after cycling were studied using field emission scanning electron microscopy (FE-SEM; JEOL, JSM-7800F, Japan) with energy dispersive X-ray spectroscopy (EDS; JEOL, Soft X-ray Emission Spectrometer). The color percentage of the EDS profile was classified using software (Cool PHP Tools, Image Color Extract, USA).

Results and Discussion

Fabrication and Characterization of the Electrodes

A p-Cu foam (PDMS-coated Cu foam) was fabricated to induce lithium deposition from the bottom of the electrode and alleviate dendrite formation. The fabrication process and SEM images of the Cu foam and p-Cu foams are presented in Scheme 1 and Fig. 1. Previous studies have shown that strong hydrogen evolution can be induced by applying a high reduction current to copper [31–36]. During Cu electrodeposition, the hydrogen bubble acts as a template and expels out simultaneously. Thus, Cu foam with a vertical hole enclosed by a thorny bush wall appeared, as shown in Fig. 1 and Fig. S1a–f. After preparing the Cu foam, the PDMS solution was cured for 72 h on a cover glass and transferred to the Cu

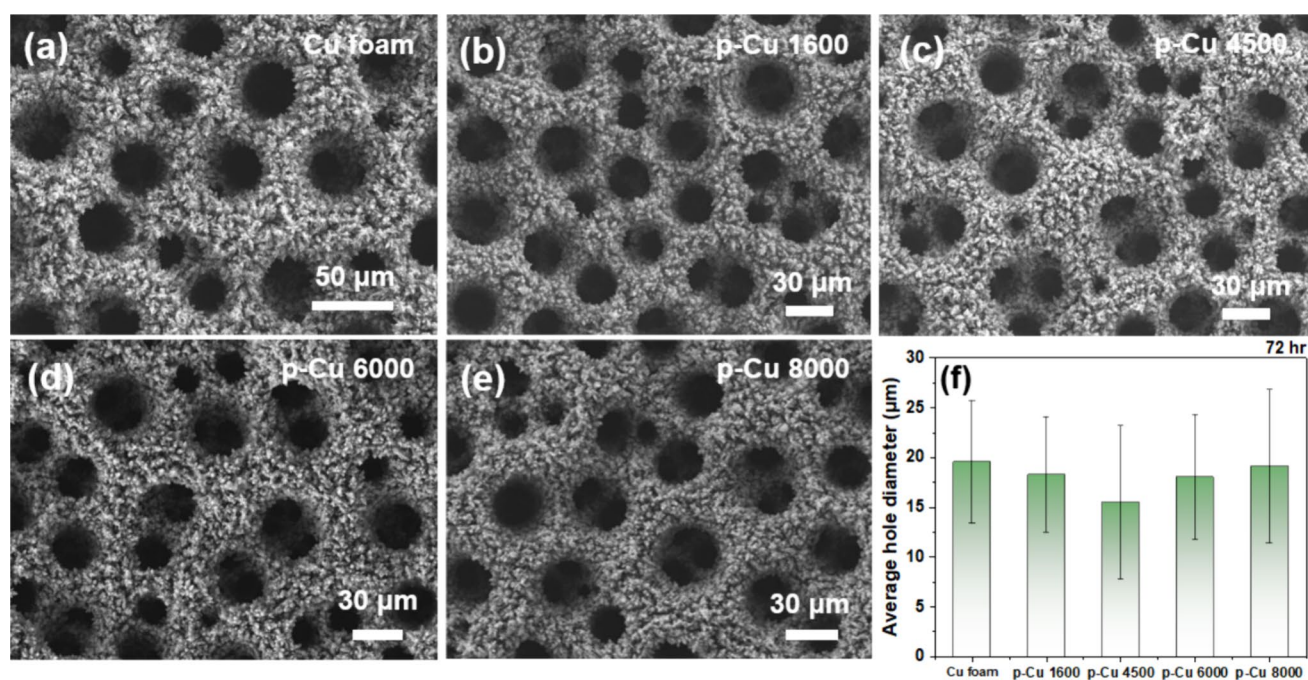


Fig. 1 a–e FE-SEM images and **f** average hole diameter of Cu foam, p-Cu 1600, 4500, 6000, and 8000

foam (Scheme 1). The amount (thickness) of polymer was controlled by regulating the spin speed of the cover glass at 1600, 4500, 6000, and 8000 rpm.

The p-Cu foam electrodes demonstrated similar average hole size and size distribution to Cu foam with diameters of 10–25 μm, as shown in Fig. 1, Fig. S1, and Fig. S2. Here, we have measured the size of approximately 100 holes in the images using a graphic program of ImageJ. The result indicates that the PDMS coating process does not damage the structure of the Cu foam. In addition, the p-Cu foam samples displayed a uniform dispersion of PDMS only on the surface of a thorny bush wall of the Cu foam regardless

of spin speed, as shown in Fig. 2. The PDMS did not block the vertical holes, creating a pathway for the electrolyte. It appears that some of them do not have a vertical hole in the cross-section, but this is due to the cutting position. Figure S1f–j, Fig. S3, and Fig. 2g–j clearly demonstrate that the pores formed inside the thorny bush wall of p-Cu foams were filled, and the top of the wall was covered with PDMS. The relative amount of Si corresponding to PDMS was investigated by EDS, and the results are summarized in Table. S1. The relative amount of PDMS was inversely proportional to the rotation speed, indicating that the thickness of PDMS decreased with increasing rotation speed. The amount of Si

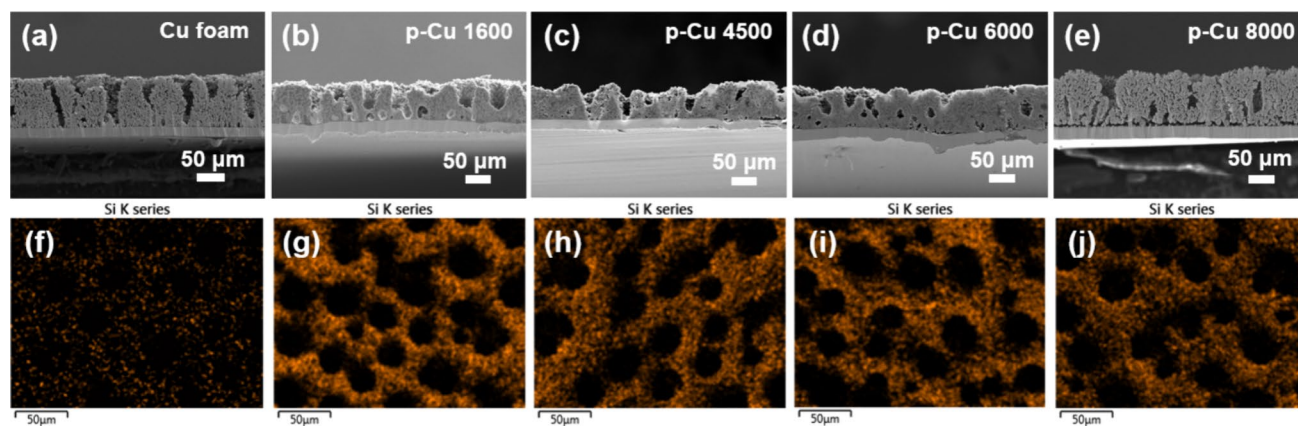


Fig. 2 a–e Cross-sectional SEM images and **f–j** surface EDS spectra of Cu foam, p-Cu 1600, 4500, 6000, and 8000

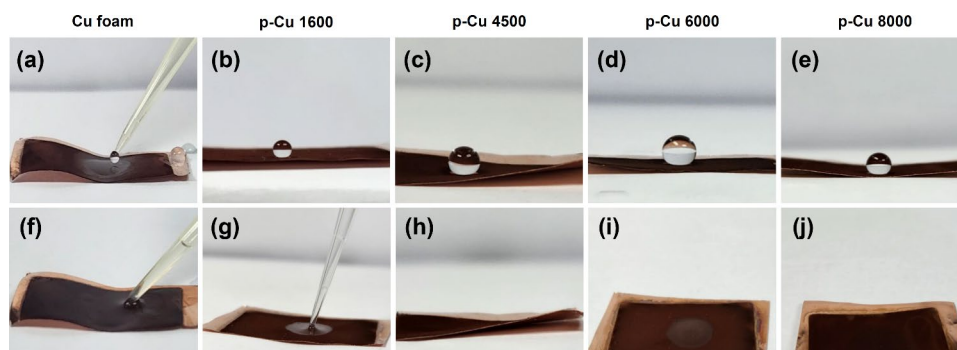
was 22.2%, 11.93%, 6.99%, and 6.5% for p-Cu 1600, 4500, 6000, and 8000, respectively. This was more clearly verified by the increase in the sample weight after PDMS coating, as shown in Table 1. The weight reduced from 22.7 to 16.5 mg, 7.6 mg, and 5.7 mg as rotation speed increased from 1600 to 8000 rpm. The relative amount of PDMS was also studied by calculating the area ratio of orange (Si from PDMS) to black using graphical software, as shown in Table. S2. This showed a similar trend to the data obtained from the EDS and weight measurements. These results indicate that the coating process can be easily applied with reasonable quality while controlling the thickness of PDMS.

To investigate whether the PDMS coating disturbs the access of the electrolyte to the electrode, the surface wettability of the Cu foam and p-Cu foams was studied by dropping water or an organic electrolyte (the same electrolyte used for the electrochemical study; DME:DOL = 8:2 + 1.0 M LiTFSI) onto the electrode, as shown in Fig. 3. As the electrode was not sufficiently flat to analyze the contact angle, photographs are provided in the figure. When the water droplet was dropped on the Cu foam, it was soaked into the electrode due to the capillary force and hydrophilicity of the electrode (Fig. 3a). Meanwhile, the p-Cu foams demonstrated impressive hydrophobicity, as shown in Fig. 3b–e, even though the main pores were not blocked by PDMS, as already shown in Figs. 1 and 2. This high hydrophobicity also supports the idea that PDMS uniformly wraps around the top of the wall. In contrast to water, organic electrolyte demonstrated the opposite phenomena. Regardless of surface status, the organic electrolyte soaked in the Cu foam from Cu foam to various p-Cu foams, as shown in Fig. 3f–j.

Table 1 Weight of samples after Cu foam deposition and PDMS transfer process

Weight	p-Cu 1600	p-Cu 4500	p-Cu 6000	p-Cu 8000
Cu foil	0.1475 g	0.1461 g	0.1451 g	0.1478 g
Cu foam	0.1724 g	0.1703 g	0.1719 g	0.1750 g
p-Cu foam	0.1951 g	0.1868 g	0.1795 g	0.1807 g
Transferred PDMS	+22.7 mg	+16.5 mg	+7.6 mg	+5.7 mg

Fig. 3 a–e Water droplet images and f–j organic electrolyte droplet images on Cu foam, p-Cu 1600, 4500, 6000, and 8000



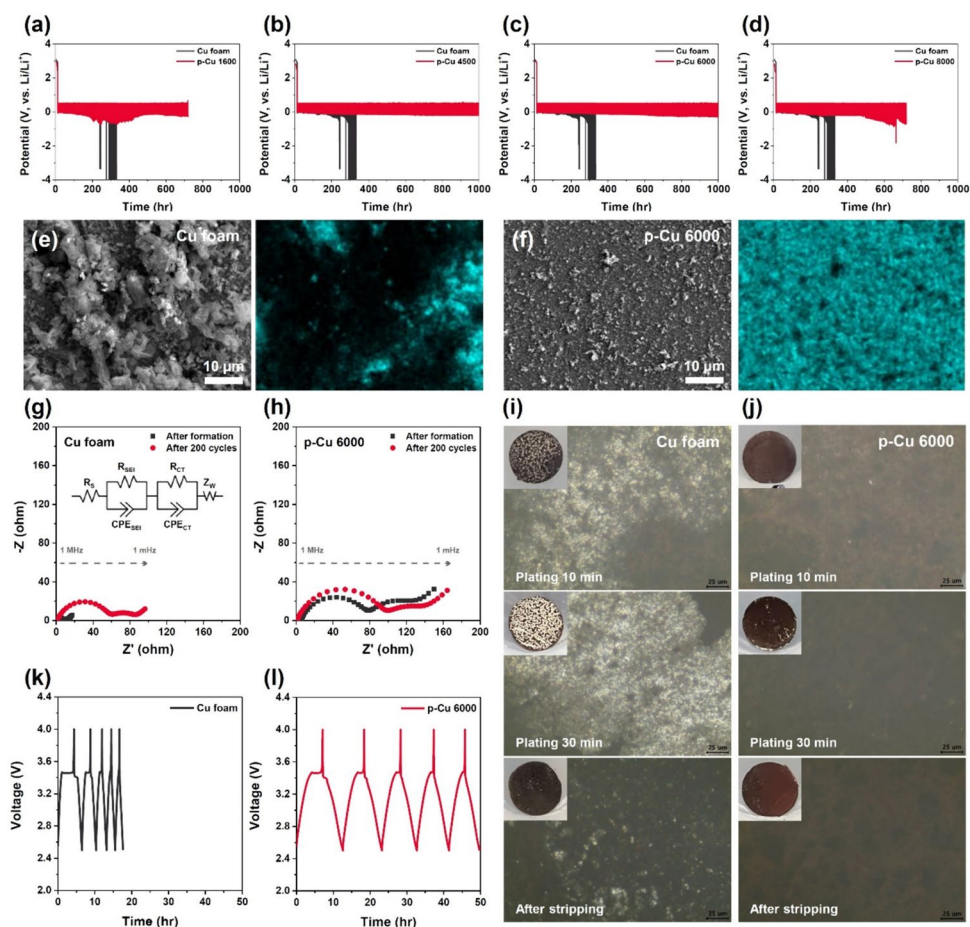
From this result, it can be inferred that the PDMS did not interrupt the access of the organic electrolyte to the current collector during the electrochemical reaction.

Coin Cell Experiment

The electrochemical behavior of the Cu foam/Li metal half-cell is shown in Fig. 4a–d. The Cu foam electrode exhibited severe polarization after 200 h; even after 400 h, cycling of the cell with Cu foam was halted. It is considered that sudden failure cycling of the cell with Cu foam might be attributed to the formation of dendritic Li at the Cu foam anode, where the current distribution cannot be controlled well during the electrochemical process [37, 38]. In contrast, the p-Cu foam showed stable Li plating/stripping behaviors; although p-Cu 8000 showed fading of cycling after 700 h, the polarization of the cells with p-Cu 4500 and 6000 remained well even after 700 h, indicating that Li plating/stripping was well controlled at the Cu foam interfaces. Comparing the potential profiles between the first and 60th cycle also provided meaningful clues for estimating the effectiveness of the p-Cu foam (Fig. S4). In the first cycle, the Cu foam and p-Cu 6000 showed similar potential Li plating/stripping curves, while the p-Cu foam exhibited a slightly increased Li plating/stripping capacity (Cu foam: 1.74 (charge)/1.62 (discharge) mA h; p-Cu 6000: 1.73 (charge)/1.70 (discharge) mA h). In contrast, the amount of Li plating/stripping in the Cu foam was markedly decreased to 0.37 mA h along with a significant overpotential (polarization; ΔV : 282.3 mV) at 60 cycles, indicating that a reversible Li plating/stripping reaction did not occur in the Cu foam. Otherwise, p-Cu 6000 still exhibited Li plating/stripping with less polarization (ΔV : 107.5 mV) even after 60 cycles, implying that the Li plating/stripping reaction was still facilitated at p-Cu 6000.

To evaluate the effectiveness of the p-Cu 6000 anode, each anode after Li plating/dissolution performance was recovered after 200 cycles, and their surface morphologies were analyzed by SEM (Fig. 4e–f). Note that there are many dendritic Li on the surface of cycled Cu foam, indicating that Li plating and dissolution mainly occurred concentrated at the surface. In the EDS analysis, only 11.8% of Cu element

Fig. 4 a–d Cycling performance of Cu foam/Li metal half-cells. FE-SEM images and EDS spectra of Cu element for e Cu foam and f p-Cu 6000. g, h Nyquist plots and microscope images of i Cu foam, and j p-Cu 6000, and k, l full-cell operation of Cu foam and p-Cu 6000



was detected at the surface, implying that most of the surface was covered by dendritic Li. In contrast, recovered p-Cu 6000 indicated relatively smooth surface morphologies, which can support that most of the Li plating and dissolution reactions occurred inside pores in the p-Cu 6000. This is consistent with EDS analysis: Cu element was detected as the main element in the recovered p-Cu 6000 (41.6%), while the recovered Cu foam showed only 11.8% of Cu at the surface. This is well harmonized with the EIS results (Fig. 4g–h). The first semicircle indicates internal resistances associated with the SEI layers (R_{SEI}), and the second semicircle implies internal resistances of charge transfer (R_{CT}) between the Cu foam and the interfaces. After the formation step, Cu foam showed lower internal resistances (R_{SEI} : 6.15 Ω , R_{CT} : 4.59 Ω) than p-Cu 6000 (R_{SEI} : 73.4 Ω , R_{CT} : 43.4 Ω) because there were no additional barriers at the interface of Cu foam, while the Li^+ migration was disturbed by additional PDMS layers at the interfaces. However, the Cu foam showed drastic increases in resistance after 200 cycles, which is almost 658.9% larger than after the formation step, which was attributed to the parasitic reaction such as electrolyte decomposition occurring at a low electrochemical potential [39, 40]. On the other hand, the p-Cu 6000

only afforded slightly increased internal resistances (15.9%) because undesired surface reactions were well controlled in the p-Cu 6000 as it effectively controls surface morphologies of the anode upon cycling.

To figure out what happens at the early step, the surface of each anode was analyzed by microscopes (Fig. 4i–j). The Li growing at the surface was well observed in the cell with Cu foam. In contrast, it was hard to observe such Li growing behaviors in the cell with p-Cu 6000, implying that the Li plating might occur in the porous sites of p-Cu 6000. When the cells were further charged, the formation of the dendritic Li was observed in the Cu foam, which indicates stable Li deposition was not well controlled at the surface. On the other hand, p-Cu 6000 still exhibited a stable surface state compared to the Cu foam, implying that the PDMS-based functionalization would be effective for controlling Li deposition behaviors even at high charging currents.

To estimate the effectiveness of p-Cu 6000, a pre-cycled p-Cu 6000 anode (after 50 cycles of Li plating/stripping) was recovered and cycled with the LFP cathode. As shown in Fig. 4k–l, the cell with the cycled p-Cu 6000 and LFP exhibited stable cycling behavior; the cycled p-Cu 6000 served as a good host for Li plating/stripping, thereby the

LFP cathode showed stable cycling retention. In contrast, a narrow voltage–time curve was observed for the cycled Cu foam. Note that cycling was completed in less than 20 h, indicating that much less Li was utilized in the cycled Cu foam. This indicates that the untreated Cu foam anode cannot sufficiently provide Li^+ in the cell, leading to a fast decay in the cycling retention of the LFP cathode. In particular, the coulombic efficiency of the p-Cu 6000 indicated 90.6% after 5 cycles, while the Cu foam only showed 83.7% of the coulombic efficiency, indicating that once PDMS was coated on the Cu foam, it may improve the current distribution at the anode interface, thereby resulting in stable cycling behavior of Li plating/stripping.

Conclusion

In this study, we fabricated a PDMS-coated 3D-porous Cu foam electrode using hydrogen bubbles as a template for use as an anode electrode in LMBs. PDMS with different thicknesses was coated on 3D-porous Cu foam by varying the speed of the spin coater. Through this simple fabrication process, we uniformly and conveniently coated the polymer on the Cu foam without deforming its porous structure of Cu foam. The PDMS successfully covered the top of the Cu foam without preventing the electrolyte from accessing the current collector. The prepared samples exhibited a consistent pore size of approximately 20 μm without any pores being blocked by PDMS. As the spin speed increased, the amount of PDMS loaded decreased, with the optimal condition being at 6000 rpm, where 7.6 mg of PDMS was loaded. The p-Cu foam electrodes exhibited superior durability in the half-cells, as they exhibited stable Li plating/stripping behaviors for 1000 h, whereas the cell with Cu foam displayed severe polarization even after 200 h. This is because the functionalized PDMS layer at the interface of the Cu foam prevented dendritic Li formation during the discharge process. When the cycled PDMS-functionalized Cu foam was combined with the LFP cathode, it exhibited stable cycling behavior, while the recovered Cu foam exhibited fast-decaying cycling retention even after 20 h. These results indicate that the PDMS-coated 3D-porous Cu foam electrode is an advanced anode that allows reversible Li deposition/dissolution, not only limited to conventional LIBs but also expanded to advanced batteries that employ Li metal anodes.

Acknowledgements This work was supported by the Core Research Institute (CRI) Program, the Basic Science Research Program through the National Research Foundation of Korea (NRF), Ministry of Education (NRF-2017R1A6A1A06015181). This work was also supported by the Industrial Strategic Technology Development Program (20010488, Development of 16 μm pitch double sided COF materials and process

technology UHD display) funded by the Ministry of Trade, Industry, and Energy (MOTIE, Korea).

Author Contributions Jihyeok Song: Methodology, validation, formal analysis, investigation, writing—original draft, visualization. Subin Lee: Validation, formal analysis, investigation, writing—original draft. Youngkwang Kim: Conceptualization, writing—original draft. Yung-Eun Sung: Supervision. Taeun Yim: Conceptualization, writing—original draft, writing – review and editing, supervision, project administration, funding acquisition. Oh Joong Kwon: Conceptualization, writing—original draft, writing—review and editing, supervision, project administration, funding acquisition.

Data Availability Data will be made available on request.

Declarations

Conflict of Interest The authors declare no conflicts of interest.

References

1. X.B. Cheng, R. Zhang, C.Z. Zhao, F. Wei, J.G. Zhang, Q. Zhang, *Adv. Sci.* **3**, 1500213 (2015)
2. X.B. Cheng, R. Zhang, C.Z. Zhao, Q. Zhang, *Chem. Rev.* **117**, 10403–10473 (2017)
3. D. Lin, Y. Liu, Y. Cui, *Nat. Nanotechnol.* **12**, 194–206 (2017)
4. B. Zhu, Y. Jin, X. Hu, Q. Zheng, S. Zhang, Q. Wang, J. Zhu, *Adv. Mater.* **29**, 1603755 (2017)
5. X.Q. Zhang, X.B. Cheng, X. Chen, C. Yan, Q. Zhang, *Adv. Funct. Mater.* **27**, 1605989 (2017)
6. E. Markevich, G. Salitra, F. Chesneau, M. Schmidt, D. Aurbach, *ACS Energy Lett.* **2**, 1321–1326 (2017)
7. D. Lin, J. Zhao, J. Sun, H. Yao, Y. Liu, K. Yan, Y. Cui, *Proc. Natl. Acad. Sci. U.S.A.* **114**, 4613–4618 (2017)
8. K.N. Wood, E. Kazyak, A.F. Chadwick, K.H. Chen, J.G. Zhang, K. Thornton, N.P. Dasgupta, *A.C.S. Cent. Science* **2**, 790–801 (2016)
9. J. Lang, Y. Long, J. Qu, X. Luo, H. Wei, K. Huang, H. Zhang, L. Qi, Q. Zhang, Z. Li, H. Wu, *Energy Storage Mater.* **16**, 85–90 (2019)
10. R. Xu, X.Q. Zhang, X.B. Cheng, H.J. Peng, C.Z. Zhao, C. Yan, J.Q. Huang, *Adv. Funct. Mater.* **28**, 1705838 (2018)
11. G. Zheng, C. Wang, A. Pei, J. Lopez, F. Shi, Z. Chen, A.D. Sendek, H.W. Lee, Z. Lu, H. Schneider, M.M. Safont-Sempere, S. Chu, Z. Bao, Y. Cui, *ACS Energy Lett.* **1**, 1247–1255 (2016)
12. Y. Gao, Y. Zhao, Y.C. Li, Q. Huang, T.E. Mallouk, D. Wang, *J. Am. Chem. Soc.* **139**, 15288–15291 (2017)
13. J. Luo, C.C. Fang, N.L. Wu, *Adv. Energy Mater.* **8**, 1701482 (2018)
14. X.B. Cheng, H.J. Peng, J.Q. Huang, F. Wei, Q. Zhang, *Small* **10**, 4257–4263 (2014)
15. X. Zhang, X. Chen, R. Xu, X. Cheng, H. Peng, R. Zhang, J. Huang, Q. Zhang, *Angew. Chem.* **129**, 14395–14399 (2017)
16. X. Liang, Q. Pang, I.R. Kochetkov, M.S. Sempere, H. Huang, X. Sun, L.F. Nazar, *Nat. Energy* **2**, 17119 (2017)
17. C. Yan, X.B. Cheng, Y. Tian, X. Chen, X.Q. Zhang, W.J. Li, J.Q. Huang, Q. Zhang, *Adv. Mater.* **30**, 1707629 (2018)
18. G. Zheng, S.W. Lee, Z. Liang, H.W. Lee, K. Yan, H. Yao, H. Wang, W. Li, S. Chu, Y. Cui, *Nat. Nanotechnol.* **9**, 618–623 (2014)
19. S. Sen Chi, Y. Liu, W.L. Song, L.Z. Fan, Q. Zhang, *Adv. Funct. Mater.* **27**, 1700348 (2017)

20. X.B. Cheng, H.J. Peng, J.Q. Huang, R. Zhang, C.Z. Zhao, Q. Zhang, *ACS Nano* **9**, 6373–6382 (2015)
21. D. Lin, Y. Liu, Z. Liang, H.W. Lee, J. Sun, H. Wang, K. Yan, J. Xie, Y. Cui, *Nat. Nanotechnol.* **11**, 626–632 (2016)
22. J.H. Um, M. Choi, H. Park, Y.H. Cho, D.C. Dunand, H. Choe, Y.E. Sung, *Sci. Rep.* **6**, 18626 (2016)
23. C.P. Yang, Y.X. Yin, S.F. Zhang, N.W. Li, Y.G. Guo, *Nat. Commun.* **6**, 8058 (2015)
24. J.H. Um, H. Park, Y.H. Cho, M.P.B. Glazer, D.C. Dunand, H. Choe, Y.E. Sung, *RSC Adv.* **4**, 58059–58063 (2014)
25. Y. Liu, D. Lin, Z. Liang, J. Zhao, K. Yan, Y. Cui, *Nat. Commun.* **7**, 10992 (2016)
26. H. Qiu, T. Tang, M. Asif, X. Huang, Y. Hou, *Adv. Funct. Mater.* **29**, 1808468 (2019)
27. Y. Kim, S. Jeong, H.E. Bae, A. Tron, Y.E. Sung, J. Mun, O.J. Kwon, *Int. J. Energy Res.* **45**, 10738–10745 (2021)
28. Y. Shi, Z. Wang, H. Gao, J. Niu, W. Ma, J. Qin, Z. Peng, Z. Zhang, *J. Mater. Chem. A.* **7**, 1092–1098 (2019)
29. J. Yun, B.K. Park, E.S. Won, S.H. Choi, H.C. Kang, J.H. Kim, M.S. Park, J.W. Lee, *ACS Energy Lett.* **5**, 3108–3114 (2020)
30. S. Li, J. Zhang, J. He, W. Liu, Y.H. Wang, Z. Huang, H. Pang, Y. Chen, *Adv. Sci.* **10**, 2304506 (2023)
31. Y. Li, W.Z. Jia, Y.Y. Song, X.H. Xia, *Chem. Mater.* **19**, 5758–5764 (2007)
32. B.J. Plowman, L.A. Jones, S.K. Bhargava, *Chem. Commun.* **51**, 4331–4346 (2015)
33. Y.S. Park, W.S. Choi, M.J. Jang, J.H. Lee, S. Park, H. Jin, M.H. Seo, K.H. Lee, Y. Yin, Y. Kim, J. Yang, S.M. Choi, *ACS Sustainable Chem. Eng.* **7**, 10734–10741 (2019)
34. H. Mehrabi, S.K. Conlin, T.I. Hollis, B.S. Gattis, J. Nelson Weker, R.H. Coridan, *Energy Technol.* **11**, 2201124 (2023)
35. H. Yang, X. Hao, J. Tang, W. Jin, C. Liu, H. Hou, X. Ji, J. Hu, *Appl. Surf. Sci.* **494**, 731–739 (2019)
36. S. Vesztergom, A. Dutta, M. Rahaman, K. Kiran, I. Zelocualtecatl Montiel, P. Broekmann, *ChemCatChem* **13**, 1039–1058 (2021)
37. O. Crowther, A.C. West, *J. Electrochem. Soc.* **155**, A806 (2008)
38. L. Yu, J. Wang, Z.J. Xu, *Small Struct.* **2**, 2000043 (2021)
39. N.D. Trinh, D. Lepage, D. Aymé-Perrot, A. Badia, M. Dollé, D. Rochefort, *Angew. Chem. Int. Ed.* **57**, 5072–5075 (2018)
40. Q. Wang, B. Liu, Y. Shen, J. Wu, Z. Zhao, C. Zhong, W. Hu, *Adv. Sci.* **8**, 2101111 (2021)

Publisher's Note Springer Nature remains neutral with regard to jurisdictional claims in published maps and institutional affiliations.

Springer Nature or its licensor (e.g. a society or other partner) holds exclusive rights to this article under a publishing agreement with the author(s) or other rightsholder(s); author self-archiving of the accepted manuscript version of this article is solely governed by the terms of such publishing agreement and applicable law.